

# Two-photon reactions at high energies

H.G. Dosch<sup>a</sup>

<sup>a</sup>Inst. Theor. Physik der Universität, Philosophenweg 16, D69120 Heidelberg, Fed. Rep. Germany  
email: h.g.dosch@thphys.uni-heidelberg.de

We present a short overview over the different contributions to high energy photon photon scattering and explore the possibilities of tuning the sizes of the scattered objects by changing the virtuality of the photons. We compare the experimental data with model calculations. The difficulties with inclusive charm production are discussed.

## 1. Introduction

The reactions  $\gamma^{(*)}\gamma^{(*)} \rightarrow$  hadrons at high energies can be viewed as scattering processes of partonic systems with tunable size, since the reaction time of a highly energetic photon is short as compared to its dissoziation time into partons [?] and the size of the system depends on the virtuality of the photon. The situation is summarized in figure 1.

For high virtualities of both photons not only the parton densities in the photon can be described well by perturbative QCD but also the interaction between the small partonic systems. Therefore we have in  $\gamma^{(*)}\gamma^{(*)}$  systems the unique possibility to isolate a small angle high energy scattering process determined by perturbative QCD. This investigation is particularly interesting since it can clarify the question of the strong energy dependence at high photon virtualities observed at HERA. In deep inelastic scattering the energy dependence at fixed photon virtuality  $Q^2$  is expressed through the dimensionless Bjorken variable  $x = Q^2/(Q^2 + W^2)$  where  $W$  is the  $\gamma^{(*)}\gamma^{(*)}$  c.m. energy. There are currently two principal explanations for the strong dependence on  $1/x$  under discussion. One starts from the usual QCD evolution using renormalization group arguments to sum powers of  $\alpha_s \log(Q^2/Q_0^2)$ . Here the  $x$ -dependence cannot be predicted but there are initial conditions at fixed  $Q_0^2$  which describe the observed cross sections very well. The rapid rise of the proton structure function with small  $x$  is then explained by a singularity of the

Mellin transform of the DGLAP splitting function. On the other hand a summation of powers of  $\alpha_s \log(W^2/W_0^2)$  first performed by Lipatov and collaborators [2,3] yields a power behaviour of the total cross section like  $(W^2/W_0^2)^{\epsilon_h}$  where to leading order  $\epsilon_h \approx \alpha_s 4 \log 2 \approx 0.55$  even for a small value  $\alpha_s = 0.2$ . If this behaviour is interpreted in the language of Regge trajectories it corresponds to a trajectory with a much higher intercept than the soft pomeron needed to describe high energy hadron hadron scattering [4]. The summation of powers of  $\alpha_s \log(W^2/W_0^2)$  is a perturbative procedure and the corresponding pomeron is called the hard pomeron or from the initial of its authors BFKL-pomeron. The BFKL formalism has been applied to  $\gamma^{(*)}\gamma^{(*)}$  scattering in [5,6].

The nice picture seemingly explaining the strong rise at small  $x$  was disturbed by the calculations in next-to-leading-order, again by Lipatov and Fadin [7] and an independent group [8]. The contributions to the intercept were as large as the ones from the leading order and reduced the intercept to a value very near to one. This clearly indicates that resummations are necessary. Attempts in this direction [9,10] lead an intercept near 1.2.

Objections have been brought forward against the DGLAP evolution, and a solution [11] which is also very successful from a phenomenological point of view has been proposed, namely the introduction of two pomerons; a soft one relevant for low  $Q^2$  with intercept 1.08 and a hard one important for high  $Q^2$  values with intercept 1.42,

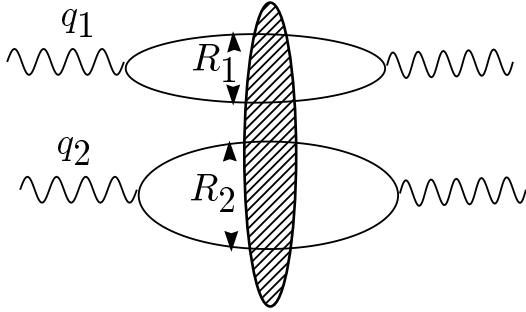


Figure 1. The diffractive contribution to hadronic  $\gamma^{(*)}\gamma^{(*)}$  scattering. The size of the quark antiquark system is inversely proportional to the virtuality:  $R_i \sim 1/Q_i = \sqrt{-q_i^2}$ .

i.e. near the leading order BFKL intercept. Since in  $\gamma^*\gamma^*$  reactions with highly virtual photons no non-perturbative input as the initial conditions of the parton distributions of the proton are needed this reaction plays a privileged role for the clarification of the nature of the energy dependence in perturbative QCD.

The experiments of LEP2 open thus a new window to investigate diffractive processes, but the kinematic range is not such as to make non-diffractive and soft diffractive contributions negligible. We put in this contribution the main emphasis on the soft diffractive contributions. They are modelled by an approach to high energy scattering and non-perturbative QCD which turned out to be successful in many reactions. The total  $\gamma^{(*)}\gamma^{(*)}$  cross section is in this description given as a superposition of the forward scattering amplitude  $T(W^2, R_1, z_1, R_2, z_2)$  of two colour-singlet quark-antiquark pairs [12] with size  $R_1$  and  $R_2$  respectively with the  $\rho_\gamma$  the quark densities in a photon (see 5) as weight factors

$$\sigma_{\gamma^*\gamma^*} = \int d^2R_1 d^2R_2 \int_0^1 dz_1 dz_2 \rho_\gamma(Q^2, R_1, z_1) \rho_\gamma(Q^2, R_2, z_2) T(W^2, R_1, z_1, R_2, z_2). \quad (1)$$

If in a scattering process one object is small and one large the variation of the amplitude with the

size of the small object can be calculated both in perturbative QCD and in non-perturbative models. They both predict a variation (apart from logarithms) of the forward scattering amplitude  $\sim R^2$  and hence  $\sim 1/Q^2$ . Therefore it is not astonishing that both perturbative and non-perturbative calculations give reasonable results also outside their domain of strict applicability. If however both objects are of equal size and small,  $R = R_1 \approx R_2$ , the behaviour is very different: in perturbative QCD the cross section is proportional to  $R^2$ , in the non-perturbative model however like  $R^4$ . This opens the aforementioned separation of the perturbative domain. But even in this case the perturbative model is useful since it allows to estimate the kinematical region where non-perturbative effects can be neglected.

As non-diffractive contributions we have the box diagram (figure 2 (a)) and the reggeon exchange, indicated in figure 2 (b).

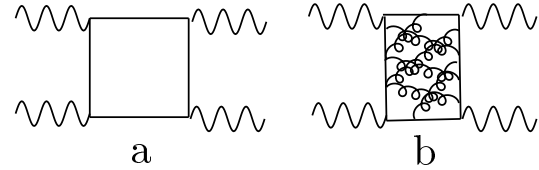


Figure 2. a: The box diagram giving rise to a fixed pole in the complex  $J$  plane. b: A schematic description of the reggeon exchange.

## 2. Non-diffractive and soft diffractive contributions to $\gamma^{(*)}\gamma^{(*)}$ scattering

The box diagram of figure 2 (a) plays a special role. For very large virtualities of the photons or high quark masses the QCD corrections to the box diagram are under control and it should not be modified by them in an essential way. In Regge language the box diagram gives rise to a fixed double pole at  $J = 0$  in the angular momentum plane. Its forward amplitude without any approximations is given in [13]. It decreases with energy

$\sim \log(W)/W^2$ , it is important at moderate energies and large virtualities.

The *reggeon exchange* has to be added to the fixpole contribution. It is perhaps the biggest source of uncertainty in the model calculations. We use the factorizing expression [13]:

$$\sigma_{\gamma^*\gamma^*}(s, Q_1^2, Q_2^2) = 4\pi^2\alpha^2 \frac{C}{A} \left(\frac{a}{Q_1^2 + A}\right)^{1-\eta} \left(\frac{A}{Q_2^2 + A}\right)^{1-\eta} \left(\frac{s}{a}\right)^{-\eta_{\text{nb}}} \quad (2)$$

with  $A = 0.3 \text{ GeV}^2$ ,  $C = 0.38$ , and  $\eta = 0.45$ . It shows the typical energy behaviour of the exchange of the reggeon trajectory.

In the limit of one the photon virtualities  $Q^2$  going to zero it agrees for  $x \geq 0.1$  very well with the hadronic photon structure function related to the DGLAP evolved pion structure function by naive VDM. It might somewhat overestimate the reggeon contribution at small virtualities: If it is extrapolated to  $\gamma\gamma$  scattering the Regge-contribution to  $\sigma_{\gamma\gamma}$  is about a factor 3 larger than expected from factorization and the values obtained in [11].

The *soft diffractive contribution* is evaluated in an approach [14] to high energy scattering particularly suited to incorporate non-perturbative aspects of QCD. The non-perturbative behaviour of QCD is treated in the model of the stochastic vacuum [15,16]. It is based on the assumption that the infrared behaviour of QCD can be approximated by a Gaussian stochastic process in the gluon field strength. With this assumption one can evaluate the expectation value of Wegner-Wilson loops and one obtains confinement for non-Abelian theories. Although the model was originally formulated in Euclidean space-time it can be extended to describe the expectation value of two Wegner-Wilson loops in Minkowski space with lightlike sides [12,17,18]. In this way one obtains the non-perturbative contribution to the scattering amplitude of two quark-antiquark pairs.

The cross section for scattering of quark-antiquark pairs with sizes  $R_1$  and  $R_2$  respectively obtained from this model can be approximated to a reasonable accuracy (10-15 %) by the following

simple factorizing formula:

$$\sigma_{dip\ dip}(R_1, R_2) = 0.7 \frac{\langle g^2 FF \rangle^2}{4\pi^2} R_1 R_2 \times \left(1 - \exp\left(-\frac{R_1}{3.1 a}\right)\right) \left(1 - \exp\left(-\frac{R_2}{3.1 a}\right)\right) \quad (3)$$

where  $\langle g^2 FF \rangle$  is the gluon condensate [19], and  $a$  the correlation length of the gauge invariant gluon field strength correlator, the numerical values are given below in equation 4

As can be seen from this equation the model depends essentially on two typically non-perturbative parameters, which specify the Gaussian process mentioned above: the strength of the gluon correlator given through the gluon condensate and  $a$ , its correlation length. From these one can calculate the slope of the linear confining potential [15,16]. As it stands the model leads to cross sections which are constant with increasing energy. The parameters of the model were fine tuned by a fit to the iso-singlet exchange part of (anti-)proton-proton scattering at  $W = \sqrt{s} = 20 \text{ GeV}$ . The resulting parameters which are in the limits of the values determined by lattice calculations and also lead to the correct value of the slope of the confining potential are:

$$\langle g^2 FF \rangle = 2.49 \text{ GeV}^4 \quad a = 0.35 \text{ fm} \quad (4)$$

The phenomenologically observed increase with energy of hadronic total cross sections like  $s^{(\alpha_P-1)}$  with  $\alpha_P \approx 1.08$  [4] can be incorporated in two ways: either one lets the radius of the hadrons increase with  $s$  [17,20–22], or one takes the model as a determination of the Regge residue and adds the Regge-like increase with energy by a factor  $(W^2/W_0^2)^{(\alpha_P-1)}$  with  $W_0 = 20 \text{ GeV}$ . These two approaches give very similar results, and we adopt the latter in this paper as it is the more convenient in the present context.

Whereas hadron-hadron scattering and soft electroproduction processes (i.e. those with low photon virtuality  $Q^2$ ) can be described very well in this way, this is not the case for hard electroproduction processes where the energy ( $1/x$ ) dependence is much stronger than indicated by the soft non-perturbative pomeron with intercept  $\alpha_P = 1.08$ . As discussed in the Introduction the

occurrence of a second (hard) pomeron as proposed in [11] can explain the data in a consistent way. This two pomeron approach was adapted to the MSV model in [23] and very successfully tested for the electro- and photoproduction of vector mesons and, more relevantly here, for the proton structure function over a wide range of  $x$  and  $Q^2$ . As in [11] it was found that the soft-pomeron contribution to  $F_2$ , after an initial increase with increasing  $Q^2$ , has a broad maximum in the region of  $5 \text{ GeV}^2$  and then decreases as  $Q^2$  increases further i.e. it exhibits higher-twist like behaviour. In the context of the present model this is a consequence of the decreasing interaction strength with decreasing dipole size.

It is worth recalling the salient features of this version of the two-pomeron model which have been slightly modified for the theoretical calculations presented here, to illustrate the distinction between the soft and the hard pomeron in dipole-dipole scattering. In [23] it was assumed that all dipole amplitudes in which both dipoles are larger than the correlation length  $a = 0.35 \text{ fm}$  are dominated by the soft pomeron, and the energy dependence therefore given by  $(W^2/W_0^2)^{\epsilon_{soft}}$  with  $W_0 = 20 \text{ GeV}$  and  $\epsilon_{soft} = 0.08$ . This ensures that the hard pomeron has essentially no impact on purely hadronic scattering. If at least one of the dipoles is smaller than  $a = 0.35 \text{ fm}$  then the energy dependence is replaced by  $(W^2/W_0^2)^{\epsilon_{hard}}$  with  $\epsilon_{hard} = 0.42$ . It turned out that the model overestimated the non-perturbative contribution of very small dipoles so it was put to zero if either of the dipoles is less than  $0.16 \text{ fm}$ . With only four parameters it was possible to obtain a good description of data for the proton structure function and for the electroproduction of vector mesons without noticeably affecting earlier fits to hadron-hadron scattering.

We apply this two-pomeron model to the evaluation of the  $\gamma^{(*)}\gamma^{(*)}$  cross sections. It should be noted that the simple factorisation formula  $\sigma_{\gamma\gamma} = \sigma_{\gamma p}^2/\sigma_{pp}$  is no longer applicable in the two-pomeron situation.

The considerations outlined briefly above lead to a model for the scattering of quark-diquark dipoles on each other approximated by 3. In order to relate it to  $\gamma^{(*)}\gamma^{(*)}$  interactions we have

according to 1 to introduce the photon wave function.

The quark-antiquark density in a photon with virtuality  $Q^2 = -q_\gamma^2$  and helicity  $\lambda$  is to lowest order perturbation theory given by:

$$\begin{aligned} \rho_\gamma(\lambda = 0, Q^2, R, z) &= \frac{2N_c\alpha}{\pi^2} \hat{e}_f^2 Q^2 z^2 (1-z)^2, K_0(\epsilon R)^2 \\ \rho_\gamma(\lambda = \pm 1, Q^2, R, z) &= \frac{2N_c\alpha}{2\pi^2} \hat{e}_f^2 \times \\ &\quad \left( (z^2 + (1-z)^2) \epsilon^2 K_1(\epsilon R)^2 + m_f^2 K_0(\epsilon R)^2 \right). \end{aligned} \quad (5)$$

Here  $\hat{e}_f$  is the charge of the quark in units of the elementary charge. i.e  $\pm\frac{1}{3}$ ,  $\pm\frac{2}{3}$ ,  $m_f$  is the Lagrangian quark mass;  $\lambda = 0$  indicates a longitudinal,  $\lambda = \pm 1$  a transverse photon. The singularity of the Bessel functions at  $R = 0$  does not cause any problems, since for the evaluation of observable amplitudes the density is multiplied by the dipole cross section and the latter is proportional to  $R^2$  at small values of  $R$ , see 1 and 3. From 5

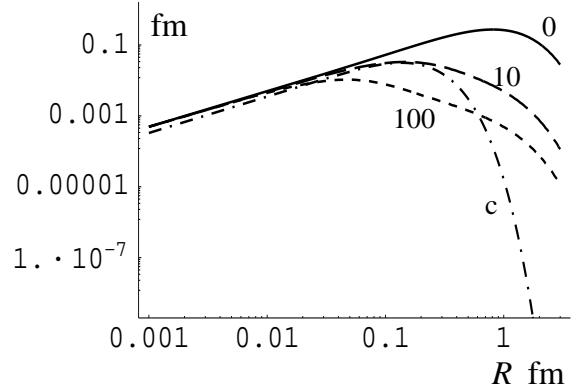


Figure 3. The quantity  $1000/\alpha R^3 \int_0^1 dz \rho_\gamma(\lambda = 1, Q^2 < R, z)$  as function of  $R$  for different values of  $Q^2$  for light quarks, solid  $\Leftrightarrow Q^2 = 0$ , long dashes  $\Leftrightarrow Q^2 = 10 \text{ GeV}^2$ , short dashes  $\Leftrightarrow Q^2 = 100 \text{ GeV}^2$ , and for charmed quarks,  $Q^2 = 0 \Leftrightarrow$  dot-dashed line.

we see that the scale is set by  $\sqrt{z(1-z)Q^2 + m_f^2}$ .

For longitudinal photons the factor  $z^2(1-z)^2$  in the density  $\rho_\gamma$  implies that the main contribution comes from the region  $z \approx \frac{1}{2}$  and the relevant scale is  $Q^2/4 + m_f^2$ . For transverse photons however the endpoints  $z = 0$ ,  $z = 1$  are not suppressed and a transverse photon might leak into the non-perturbative region even if the virtuality is quite high. This can be seen directly from figure 3.

The expressions 5 are reliable for large values of  $Q^2$  and/or large quark masses (i.e.  $c$  and  $b$ ). For small values of  $Q^2$  and light quarks the distance of the quark antiquark pair increases and confinement effects will become important. Often vector meson dominance is applied, another possibility is to introduce a constituent quark mass as infrared regularisator in the photon wave function. This approach will be justified in the following, it allows a very economical description of the photon wave function at low virtualities, which interpolates smoothly to high virtualities and even takes care of the “hard part of the photon” at low virtualities. This is especially relevant for photon-photon interactions.

Let us begin with a model investigation [24] with scalar photons and quarks. In such a case the “photon”-wave function at high virtualities is given by:

$$\begin{aligned}\tilde{\psi}_\gamma(\vec{k}_\perp) &= \frac{1}{\vec{k}_\perp^2 + z(1-z)Q^2 + m_f^2} \\ \psi_\gamma(\vec{R}) &= \frac{1}{2\pi} K_0(\sqrt{z(1-z)Q^2 + m_f^2} R) \quad (6)\end{aligned}$$

For low  $Q^2$  we expect confinement to modify these perturbative expressions considerably.

The structure of 6 is the same as that of a non-relativistic Greens function for the relative motion of a free two body system with reduced mass  $m$

$$G_0(\vec{R}, 0, M) = \frac{m}{\pi} K_0(\sqrt{2mM} |\vec{R}|), \quad (7)$$

where  $mM = -mE$  stands for the virtuality  $Q^2$ .

In order to impose confinement we go from the free particle state to a system hold together by a harmonic oscillator potential. As has been pointed out in reference [19] the harmonic oscillator is a very useful model for QCD: it shows

both confinement and asymptotic freedom. We therefore investigate the effects of confinement by comparing the free Greens function 7 with that of the full harmonic oscillator

$$G_H(\vec{R}, 0, M) = \sum_{n_1, n_2} \frac{\psi_{\vec{n}}(\vec{R}) \psi_{\vec{n}}(\vec{R})}{(n_1 + n_2 + 1)\omega + M} \quad (8)$$

which can be calculated easily.

As has been shown in [24] a free Greens function with a  $M$ -dependent shift:  $M \rightarrow M + s(M)$  yields an excellent fit to the exact Greens function 8 for all  $M \geq 0$ . We transfer this procedure to QCD by performing a  $Q^2$ -dependent shift of the flavour mass  $m_f \rightarrow m_f + m(Q^2)$  in the perturbative photon wave function. The numerical value of the shift  $m(Q^2)$  can be fixed by a fit to the phenomenologically known vector-current two-point function and thus no new parameter is introduced. The following linear parametrizations can be used

$$\begin{aligned}m_{u,d} &= \begin{cases} m_0 (1 - \frac{Q^2}{1.05}) & : Q^2 \leq 1.05 \\ 0 & : Q^2 \geq 1.05 \end{cases} \quad (9) \\ m_s &= \begin{cases} 0.15 + 0.16 (1 - \frac{Q^2}{1.6}) & : Q^2 \leq 1.6 \\ 0.15 & : Q^2 \geq 1.6 \end{cases} \\ m_c &= 1.3\end{aligned}$$

The parameter  $m_0$  for the  $u, d$  quarks was found to be  $m_0 = 0.21 \pm 0.015$  GeV. We see that above 1.05 for light quarks and 1.6 for strange quarks the current mass can be used. For charmed quarks the perturbative expression as it stands can be taken.

The densities for transverse photons integrated over the longitudinal momentum fraction  $z$  and multiplied by 1000  $R^3$  are shown in figure 3. The longitudinal photons are more concentrated at small separations  $R$  as explained above.

### 3. Results

#### 3.1. Total cross sections [13]

We first discuss the results for the total cross section of real  $\gamma\gamma$  scattering. Using the mass  $m_q = 0.21$  GeV  $m_s = 0.31$  GeV  $m_c = 1.3$  GeV we obtain the cross sections given in figure 4. The experimental cross section shows an increase with energy which is distinctly stronger than for

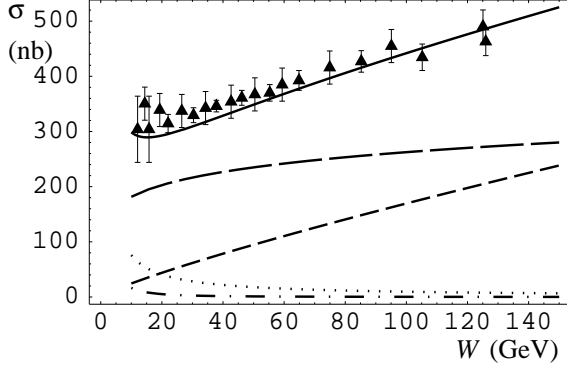


Figure 4. Cross section (nb) for  $\gamma\gamma$  scattering as function of the c.m. energy  $W$  (GeV) compared with L3 data. L3: Triangles [25] The solid curve is our model without adjusted parameters. It consists of the following contributions: soft pomeron  $\Leftrightarrow$  long dashes; hard pomeron  $\Leftrightarrow$  short dashes; fixed pole (box)  $\Leftrightarrow$  dot-dashes; reggeon  $\Leftrightarrow$  dots.

hadron hadron scattering. Our model reproduces this result and it can be explained very naturally. The singularity of the photon density  $\rho_\gamma$  at  $R = 0$  which reflects the pointlike coupling of the photon to the quark-antiquark pair gives in  $\gamma\gamma$  scattering a stronger weight to smaller dipoles in hadron hadron scattering. Since small dipoles couple to the hard pomeron which has a considerably larger intercept we obtain an overall energy dependence which is stronger than for hadrons. The contribution of the box diagram (dot-dashes in figure 4) and the reggeon exchange (dots) are of minor importance above  $W = 30$  GeV. As expected from the discussion in the introduction the purely non-perturbative model decreases much to fast with virtuality if both photons have approximately equal values for  $Q^2$ . This can be seen in figure 5 where the  $Q^2$  dependence of the total  $\gamma^{(*)}\gamma^{(*)}$  cross section is displayed as a function of  $Q^2 = \langle Q_1^2 \rangle = \langle Q_2^2 \rangle$  at the fixed c.m. energy  $W \approx 20$  GeV; at  $Q^2 = 14$  GeV<sup>2</sup> the non-perturbative contribution is negligible. The energy dependence of the  $\gamma^{(*)}\gamma^{(*)}$  cross section at  $Q^2 = 3.5$  and 14 GeV<sup>2</sup> is shown in figure 6. If the

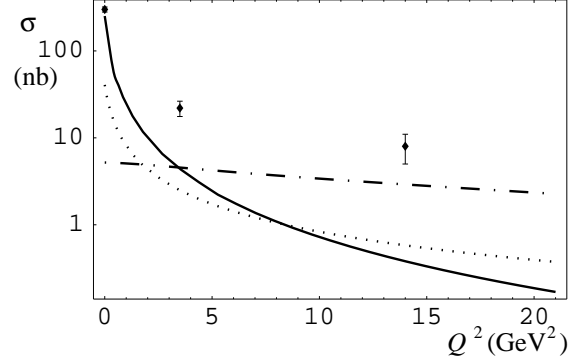


Figure 5. Cross section (nb) for  $\gamma^*\gamma^*$  scattering as function of the average photon virtuality  $\langle Q^2 \rangle = \langle Q_1^2 \rangle = \langle Q_2^2 \rangle$  (GeV<sup>2</sup>) a c.m. energy  $W \approx 20$  GeV compared with L3 data. Symbols as in figure 4

theoretical non-perturbative and non-diffractive contributions are subtracted from the experimental values the resulting energy dependence can be very well described by a power behaviour  $(W^2)^\epsilon$  with  $\epsilon = 0.3 \dots 0.4$ .

### 3.2. Photon structure functions [13]

In a photon structure function one photon is real and the other one has a virtuality  $Q^2 \neq 0$ . The structure function  $F_2^\gamma$  is defined as

$$F_2^\gamma(x, Q^2) = \frac{Q^2}{4\pi^2\alpha^2} \sigma^{\gamma^*\gamma}(W, Q^2) \quad (10)$$

with  $x = Q^2/(W^2 + Q^2)$ . As mentioned in the introduction in that case both perturbative and non-perturbative QCD give the same  $Q^2$  behaviour and we see indeed in figure 7 that the non-perturbative model describes the data very well up to  $Q^2 = 20$  GeV<sup>2</sup>. In order to extrapolate nontrivially to  $Q^2 = 0$  a modified structure function  $\tilde{F}_2^\gamma = \frac{Q^2 + 0.6 \text{ GeV}^2}{Q^2} F_2^\gamma(x = \frac{Q^2}{W^2 + Q^2}, Q^2)$  has been displayed and compared with the correspondingly multiplied experimental data from different experiments. In figure 8 the photon structure function for  $Q^2 = 10$  GeV<sup>2</sup> is shown. The agreement between theory and experiment is similarly good for other virtualities.

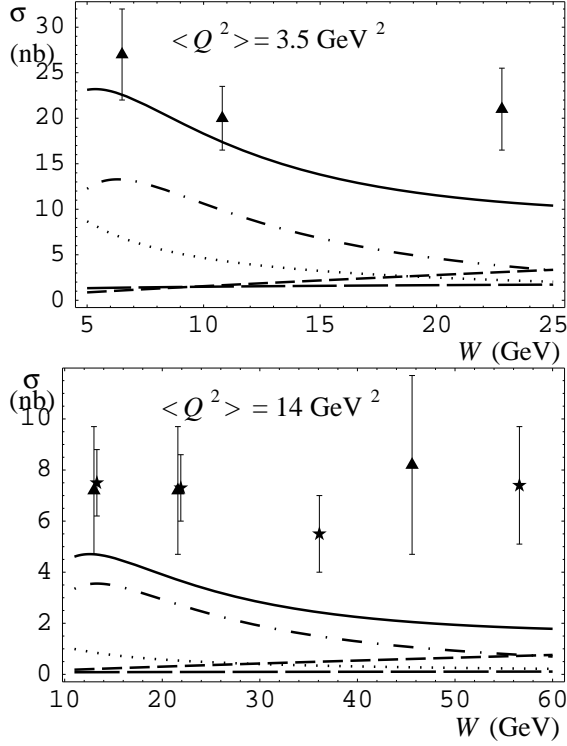


Figure 6. Cross section (nb) for  $\gamma\gamma$  scattering as function of the c.m. energy  $W$  (GeV) compared with L3 data for  $\langle Q^2 \rangle = 3.5$  and  $14 \text{ GeV}^2$  respectively. Symbols as in figure 4

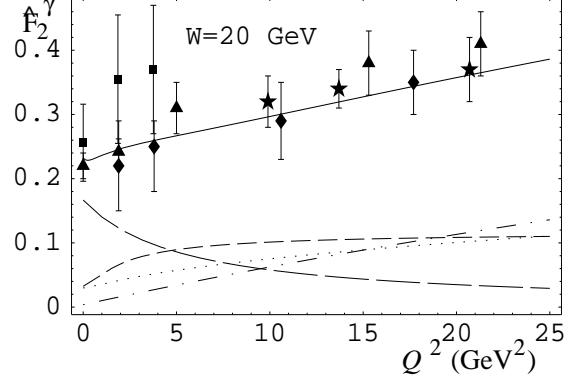


Figure 7. The modified photon structure function  $\tilde{F}_2^\gamma = (Q^2 + 0.6 \text{ GeV}^2)/Q^2 F_2^\gamma(x = Q^2/(W^2 + Q^2), Q^2)$  as function of  $Q^2$  for  $W \approx 20 \text{ GeV}$ . The data [25–27] are: Triangles  $\Leftrightarrow$  L3 ; Diamonds, Boxes  $\Leftrightarrow$  OPAL ; Stars  $\Leftrightarrow$  ALEPH The solid curve is our fit without adjusted parameters. For the different contributions see caption of figure 4.

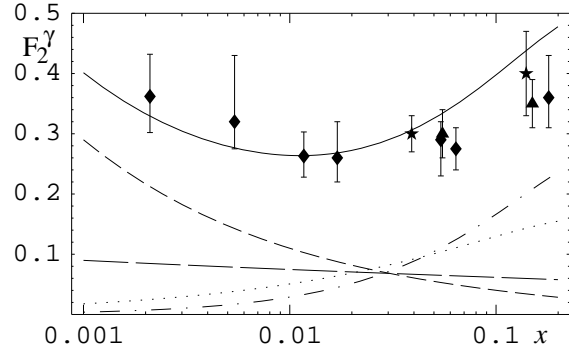


Figure 8. The photon structure function  $F_2^\gamma(x, Q^2)$  as function of  $x = \frac{Q^2}{W^2 + Q^2}$  for  $Q^2 = 10 \text{ GeV}^2$ . The data [25–27] are: Triangles  $\Leftrightarrow$  L3 ; Diamonds  $\Leftrightarrow$  OPAL ; Stars  $\Leftrightarrow$  ALEPH The solid curve is our fit without adjusted parameters. For the different contributions see caption of figure 4.

### 3.3. The reaction $\gamma^{(*)}\gamma \rightarrow c\bar{c}X$

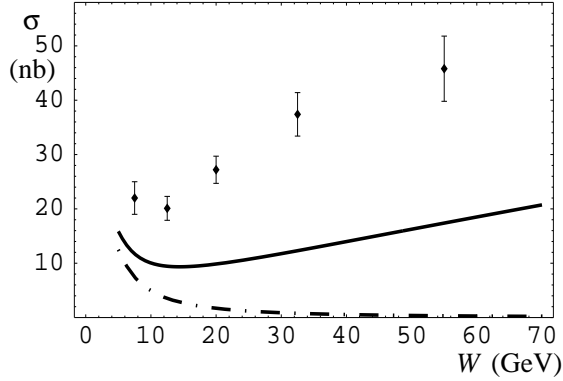


Figure 9. The cross section for the reaction  $\gamma\gamma \rightarrow c\bar{c}X$ . The solid line is the direct contribution to the structure function as predicted by the model from a picture corresponding to figure 1 and the box diagram with charmed internal quark lines (dot-dashed line); data points are from [28].

New measurements from L3 [28] and OPAL [29] yield data for inclusive charm production. In figure 9 the total cross section for the reaction  $\gamma\gamma \rightarrow c\bar{c}X$  is given. We have calculated diffractive charm production according to the physical picture of figure 1 where the quarks in the loop of photon 1 are charmed, in loop 2 all flavours are summed over and correspondingly with 1 and 2 interchanged; for the box diagram only charmed quarks contribute. We see that the theoretical values for the direct diffractive and non-diffractive production underestimate the data [28] by more than a factor two. The same happens for the case if one photon is virtual. In figure 10 the charm contribution to the photon structure function is displayed for  $\langle Q^2 \rangle = 20 \text{ GeV}^2$ . The central value of the experimental point [29] at  $\langle x \rangle = 0.02$  is again far above the theoretical value.

In principle this could indicate a failure of the model prediction for the cross section 3 for the case that one object is small and one large, but this is unlikely for the following reasons.

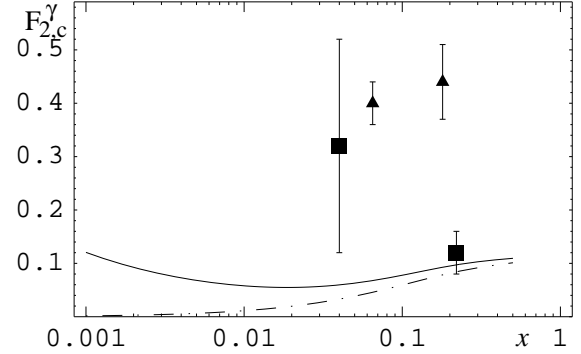


Figure 10. The photon structure function  $F_{2,c}^\gamma$  at  $\langle Q^2 \rangle = 20 \text{ GeV}^2$ . The solid line is the direct contribution to the structure function as predicted by the model from a picture corresponding to figure 1 and the box diagram with charmed internal quark lines (dot-dashed line). The boxes are the data for the charm structure function [29], the triangles are the results for the full structure function at the same average  $Q^2$ .

- 1) The charm structure function of the proton [30] agrees very well with the predictions of the model as can be seen from figure 11 and here we have the same situation of one object large and one small.
- 2) The full photon structure function at  $Q^2 = 10 \text{ GeV}^2$  is correctly predicted by the model, as can be seen from figure 8. At  $Q^2 = 10 \text{ GeV}^2$  the light quark density in a photon peaks at about the same quark-antiquark distance as a charmed pair in a real photon (see figure 3).

So we would like to conclude that there must be other mechanisms of charm production but refrain from speculations until the experimental situation especially of the charmed photon structure function is clearer.

### Acknowledgements

I thank A. Donnachie, A. Hebecker and M. Rueter for many discussions. I also want to thank



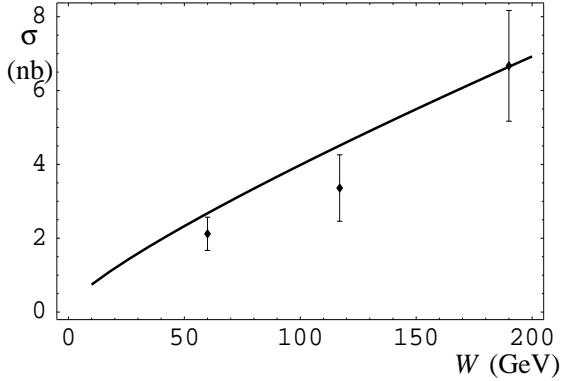


Figure 11. Cross section for the reaction  $\gamma^* p \rightarrow c\bar{c}X$ . The solid curve is our model for the direct contribution for photons with  $Q^2 = 10 \text{ GeV}^2$ . The data points are from [30]

S. Narison for having provided again the familiar and stimulating atmosphere at the QCD conference 2000 in Montpellier.

### Discussion

**S. Narison, LPMT:** *I am a bit annoyed with the  $\log(W/m_q^2)$  behaviour of the cross section when  $m_q \rightarrow 0$ . I would have expected a behaviour like  $\log(W/\mu)$  where  $\mu$  is a subtraction point. What is the meaning of  $m_q$  for light quarks?*

**H.G. Dosch:** For real photons the box diagram has an infrared singularity which is regularized by the quark mass. The same happens for the pomeron exchange of real photon photon scattering. Here the IR singularity leads to  $1/m_q^4$ ! For light quarks an IR regularization procedure has to be introduced which at the present state of the art is model dependent.

**A. Brandenburg:** *Could you explain in more detail how you obtained the quark mass that regularized the photon wave function? What is the physical interpretation? Does it have anything to do with the mass parameter in the QCD Lagrangian?*

**H.G. Dosch:** The regularization of the photon wave function by an effective mass was motivated

by model investigations [24]. The values for the regularizing masses for light quarks are given in equation 9 and are close to "constituent masses". They were obtained in the following way: The second derivative of the lowest order two point function for the vector current was compared with the corresponding phenomenological expression, consisting of the  $\rho$ -pole and a continuum. The theoretical expression contains the quark mass as only free parameter and it was fixed by equating the two expressions. For  $Q^2 > 1$  the agreement could not be improved by a finite quark mass and there the Lagrangian mass can be taken, but it is of little influence anyhow. For heavy quarks the Lagrangian quark mass at the scale  $Q^2/4$  is a reliable regularizator. For a detailed discussion I refer to reference [24].

### REFERENCES

1. B. L. Ioffe *Phys. Lett.* B30:123 (1969)
2. V. S. Fadin, E. A. Kuraev, and L. N. Lipatov. *Phys. Lett.*, B60:50, 1975.
3. Ya Ya Balitskii and L N Lipatov. *Soviet Journal of Nuclear Physics*, 28:822, 1978.
4. A Donnachie and P V Landshoff. *Physics Letters*, B296:227, 1992.
5. J Brodsky, F Hautmann, and D E Soper. *Physical Review*, D56:6957, 1997.
6. M. Boonekamp, A. De Roeck, Ch. Royon, and S. Wallon. *Nucl. Phys.*, B555:540, 1999.
7. S Fadin and L N Lipatov. *Physics Letters*, B429:127, 1998.
8. G Camicin and M. Ciafaloni. *Physics Letters*, B430:349, 1998.
9. G. P. Salam. *JHEP*, 07:019, 1998.
10. M. Ciafaloni and D. Colferai. *Nucl. Phys.*, B538:187, 1999.
11. A Donnachie and P V Landshoff. *Physics Letters*, B437:408, 1998.
12. A Krämer and H G Dosch. *Phys. Lett.*, B272:114, 1991.
13. A. Donnachie, H. G. Dosch, and M. Rueter. *Eur. Phys. J.*, C13:141, 2000.
14. O Nachtmann. *Annals Phys.*, 209:436, 1991.
15. H G Dosch. *Phys. Lett.*, 190B:177, 1987.
16. H G Dosch and Yu A Simonov. *Phys. Lett.*, 205B:339, 1988.

17. H G Dosch, Erasmo Ferreira, and A Krämer. *Phys. Rev.*, D50:1992, 1994.
18. H G Dosch. In E. Ferreira et al., editor, *Hadron Physics 96*. World Scientific, 1996.
19. M A Shifman, A I Vainshtein, and V I Zakharov. *Nucl. Phys.*, B147:385, 1979.
20. Erasmo Ferreira and Flavio Pereira. *Phys. Rev.*, D56:179–183, 1997.
21. E R Berger and O Nachtmann. *Eur. Phys. J.*, C7:459, 1999.
22. Flavio Pereira and Erasmo Ferreira. *Phys. Rev.*, D61:077507, 2000.
23. Michael Rueter. *Eur. Phys. J.*, C7:233, 1999.
24. H G Dosch, T Gousset, and H J Pirner. *Phys. Rev.*, D57:1666, 1998.
25. L3 Collaboration: M.Acciari et al: *Phys. Lett.* **B408** (1997) 450  
L3 Note 2280: Submitted to *XXIX ICHEP*, Vancouver, 1998  
M.Acciari et al. L3 Note 2400 *Int. Europhys. Conf. 99*  
M.Acciari et al: *Phys.Lett.* **B453** (1999) 333 and L3 Note 2404 M.Acciari et al: *Phys.Lett.* **B436** (1998) 403 and *Phys.Lett.* **B447** (1999) 147
26. OPAL Collaboration: F.Wäckerle: *Proc. XXVIII Int. Symp. on Multiparticle Dynamics*, Frascati, 1997  
G. Abbiendi et al., to be submitted to *Europ. Phys. J. C*  
K.Ackerstaff et al.: *Phys.Lett.* **B411** (1997) 387 and *Phys.Lett.* **B412** (1997) 225 OPAL Physics Note PN389 (Preliminary)
27. ALEPH Collaboration: R.Barate et al.: *Phys. Lett.* **B458** (1999) 152  
ALEPH 99-038: EPS-HEP99 Conference, Tampere
28. L3 Collaboration L3 Note 2548
29. Opal Collaboration: G. Abbiendi et al. To appear in *Eur. Phys. J. C*
30. Zeus Collaboration: A. Breitweg et al. hep-ex/9908012